

Article

Evaluation of Microclimate Benefits Due to Cool Pavements and Green Infrastructures on Urban Heat Islands

Giulia Del Serrone , Paolo Peluso  and Laura Moretti * 

Department of Civil, Constructional and Environmental Engineering, Sapienza University of Rome,
Via Eudossiana 18, 00184 Rome, Italy

* Correspondence: laura.moretti@uniroma1.it; Tel.: +39-06-4458-5114

Abstract: Ongoing climate change is manifesting in the expansion of the urban heat island (UHI) effect. This paper evaluates the microclimate benefits of cool pavements and green infrastructures in a historical square in Rome, Italy. The ENVI-Met software enabled us to conduct a microclimatic analysis of the examined square in July 2021, through a comparison of the thermal performances of the current asphalt and sampietrini pavement (AS) with three alternatives. The proposed options are to change the existing layout to include: light concrete slabs and green furniture consisting of 5 m high trees (LC+G1), a perimeter hedge with 5 m high trees (LC+G2), and a perimeter hedge with 15 m high trees (LC+G3). The effects of the road pavements as passive countermeasures to the UHI effect are investigated in terms of air temperature (AT), mean radiant temperature (MRT), and predicted mean vote (PMV). The results show that the existing asphalt pavement is the worst option, while the cool pavement integrated with vegetation is greatly beneficial to human thermal comfort. Compared to the current layout, LC+G3 is the best scenario, because it implies an AT reduction higher than 3 °C, a MRT reduction equal to 50%, and a maximum PMV value equal to 2.2.

Keywords: urban heat island; climate change; microclimate analysis; ENVI-Met; cool pavements; green infrastructures; predicted mean vote; mean radiant temperature



Citation: Del Serrone, G.; Peluso, P.; Moretti, L. Evaluation of Microclimate Benefits Due to Cool Pavements and Green Infrastructures on Urban Heat Islands. *Atmosphere* **2022**, *13*, 1586. <https://doi.org/10.3390/atmos13101586>

Academic Editor:
Giridharan Renganathan

Received: 27 August 2022
Accepted: 26 September 2022
Published: 28 September 2022

Publisher's Note: MDPI stays neutral with regard to jurisdictional claims in published maps and institutional affiliations.



Copyright: © 2022 by the authors. Licensee MDPI, Basel, Switzerland. This article is an open access article distributed under the terms and conditions of the Creative Commons Attribution (CC BY) license (<https://creativecommons.org/licenses/by/4.0/>).

1. Introduction

In the past few years, climate change has had several negative effects, such as changing the weather patterns and disrupting the natural balance of Earth's climate system [1]. Anthropological analyses of this phenomenon have discovered the dual role of mankind, both responsible for and a victim of global warming [2,3]. Humans are responsible for the transformation of rural areas into badly planned and designed urban areas [4,5], resulting in a large amount of energy consumption and a consequent increase in pollution [6,7]. The frequent use of artificial materials and the increase in anthropogenic heat propagation favor the development of urban heat islands (UHIs) [8,9]. They are mainly characterized by urban surfaces (e.g., roads, parking lots, pavements, and roofs) made of waterproof materials [10] with high thermal capacities. These materials absorb solar radiation throughout the day, store it in the form of thermal energy, and emit it at night [11–13]. As a result, air temperatures rise from 1 °C to 10 °C [8,14] over 24 h, negatively affecting the psychophysical comfort of people, who try to counteract high temperatures with higher electricity consumption (i.e., air conditioning), causing further deterioration of the environment and the ecosystem [15]. In the literature, urban green infrastructures (UGI), building materials (for both road pavements and factories), public transport, water treatment, and urban ventilation are the key factors that affect an urban microclimate [16–19]. Therefore, the scientific literature is investigating the best strategies to counteract and mitigate the effects of UHIs [20–22]. For example, cool pavements can soften the negative effects of UHIs through different technologies [23–25]. Furthermore, permeable pavements guarantee rainwater penetration and evaporation during the hottest hours [26,27]. In addition, in

parking areas, grass grid pavers combine both technologies for cooling the pavement and air [28–30]. Several other studies have demonstrated that the substitution of traditional asphalt pavements with cool ones has beneficial effects in terms of air temperature (AT), mean radiant temperature (MRT), and predicted mean vote (PMV). Specifically, AT reductions of about 5 °C are observed by [31,32], while for MRT an absolute decrease of about 15 °C [33] or a percentage decrease of 10% in summer and 80% in winter can occur [34]. Moreover, green areas added to cool surfaces can reduce the perceived temperatures and lead to comfortable PMV values [35,36].

Due to the recent Italian standard for the promotion of the minimum environmental criteria (CAM) [37], such measures are mandatory for all public construction works. Therefore, the authors propose a study to identify the best cool pavement to replace existing road asphalt ones. The study area is St. Peter in Chains' square, in the historic center of Rome. In [38,39], the authors carried out microclimatic analyses in the same area and demonstrated the effectiveness of some different cool pavements in terms of PMV and AT values throughout the year. Due to urban planning restrictions and landscaping which constrain the design choices, light concrete slabs or a total grass layer in the parking area gave the best results, suggesting that an even greater UHI mitigation can be obtained by combining these two solutions, and the mechanical good performances of the modular pavements cannot be overlooked [40,41]. In this paper, the authors demonstrate how the redesign of the parking area with concrete pavement combined with green furniture and trees can requalify the area. The adopted methodology is useful to achieve the objectives of human well-being and historical heritage protection in a complicated urban context. To this purpose, soft engineering and cool building materials have been merged into just one study through a scientific approach. The software ENVI-Met was used to simulate the climatic trend of the square in July 2021, which is the hottest month of the year. The results in terms of AT, MRT, and PMV allow an objective and quantitative comparison between the microclimatic conditions of the modeled scenarios. Indeed, the current layout is the worst solution, while interesting strategies with cool pavements and green infrastructures can mitigate the negative effects of climate change.

2. Materials and Methods

This article performs a microclimatic analysis in St. Peter in Chains' square in Rome (lat. 41°53'36.8"–long. 12°29'32.1"). Figure 1 shows the current layout of the square, where the parking lot has an asphalt wearing course, and the remaining surface is paved with sampietrini.



Figure 1. St. Peter in Chains' square, Rome, Italy.

The thermal properties of pavement materials play a pivotal role in the formation and manifestation of UHIs [42,43]. In particular, albedo and emissivity are the two main

parameters, as they influence the thermal behavior of the road pavement to solar irradiation [44,45]. Albedo is the ability to reflect the incident radiation [46]. It assumes values between 0 and 1, in which 0 is an ideal black surface that absorbs all incident radiation and 1 corresponds to a white surface that reflects all incident radiation [47]. Emissivity is the fraction of energy radiated compared to the one radiated by a black body; it ranges between 0 and 1, showing its resemblance to the black body. Emissivity affects surface temperatures, especially during the night, as the heat and the radiation absorbed during the day will be released into the air [48]. Instead, conductivity and thermal capacity contribute marginally to the cooling of the pavement's surface temperature. The thermal conductivity speeds up the top-down heat transfer [49], while the thermal capacity affects both the maximum and the minimum temperatures because it affects the thermal inertia [50]. According to the UHI mitigation strategies in the literature [51,52], this study takes into account the physical characteristics of the existing and the proposed road materials in Table 1 [53–55].

Table 1. Physical characteristics of the pavement materials.

Material	Albedo (-)	Emissivity (-)
Asphalt	0.2	0.9
Sampietrini	0.4	0.9
Light Concrete	0.8	0.9

Light concrete pavers substitute the existing asphalt pavement, while green furniture and trees are added to the area. Vegetation consists of a perimeter hedge and rows of trees, placed both on the perimeter and between the parking slots. Table 2 lists the thermal properties of the green elements and their heights. It also introduces transmittance, which describes the insulating capacity of a body [56].

Table 2. Physical characteristics of the green elements.

Element	Height (m)	Albedo (-)	Transmittance (W/(m ² K))
Hedge Denset	1	0.20	0.3
Deciduous Spherical Trees	5	0.18	0.3
Deciduous Spherical Trees	15	0.18	0.3

This research has been carried out with the ENVI-Met software, which evaluates the urban thermal conditions [32,34,57] through reliable outputs [58]. The software is structured on four consecutive levels. The definitions of the model and input data are in the first level, the microclimatic simulation is in the second one, and the output files are in the third one. The last level permits us to read and analyze the results using either bidimensional (2D) colored maps (Leonardo tool) [59,60] or binary output files in an ASCII format (Xtract tool) [61]. The implemented model is composed of $40 \times 30 \times 30$ grid cells, with a resolution of $2 \text{ m} \times 2 \text{ m} \times 2 \text{ m}$ (x, y, z) (Figure 2); its domain is bounded by external blue lines (existing buildings and walls) in Figure 2. It includes the central parking area, an urban road, the surrounding concrete buildings, and an existing tree. The ENVI-Met model consists of a one-dimensional limit (1D), a three-dimensional main model (3D), and a soil model. The validity and reliability of the results depend on the accuracy of the input data (i.e., local meteorological parameters, road surfaces, soil type, existing buildings, and vegetation).



Figure 2. ENVI-Met model of St. Peter in Chains' square with grid and boundaries.

In addition to the current state of the square, three scenarios with a modular light concrete pavement in the parking lot and different green furniture were implemented and simulated. Figure 3 shows all the analyzed scenarios:

1. The first scenario (AS) is the current layout, where asphalt and sampietrini compose the pavement of the parking and the carriageway, respectively (Figure 3a);
2. The second scenario (LC+G1) has light concrete slabs replacing the asphalt surface in the square and rows of 5 m high trees planted neatly in the parking lot (Figure 3b);
3. The third scenario (LC+G2) has light concrete slabs replacing the asphalt surface in the square, rows of 5 m high trees planted neatly in the parking lot, and a 1 m high hedge surrounding the area (Figure 3c);
4. The fourth scenario (LC+G3) has light concrete slabs replacing the asphalt surface in the square, rows of 15 m high trees planted neatly in the parking lot, and a 1 m high hedge surrounding the area (Figure 3d).

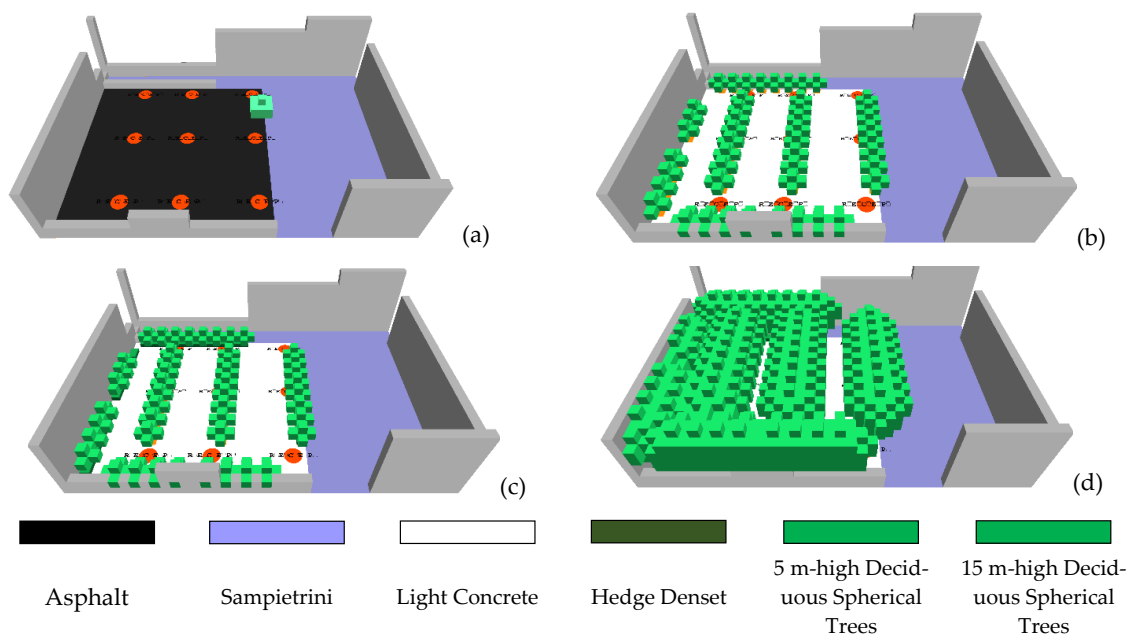


Figure 3. Scenarios implemented and analyzed with Envi-Met: (a) First scenario (AS); (b) Second scenario (LC+G1); (c) Third scenario (LC+G2); (d) Fourth scenario (LC+G3).

To carry out the simulations, the software requires input data, such as the period of analysis and the meteorological data related to the simulation time window. The microclimate analysis was carried out in July 2021, as it is the most severe month according to [39]. A 72 h analysis was performed, in which the output data were collected in the last 24 h of the simulation. The choice to perform 72 h of analysis was necessary to improve the numerical stability during the model’s spin-up phase. Figure 4 shows the variation in the air temperature and the relative humidity during the simulated day, extracted from the meteorological input data interface of the ENVI-Met software.

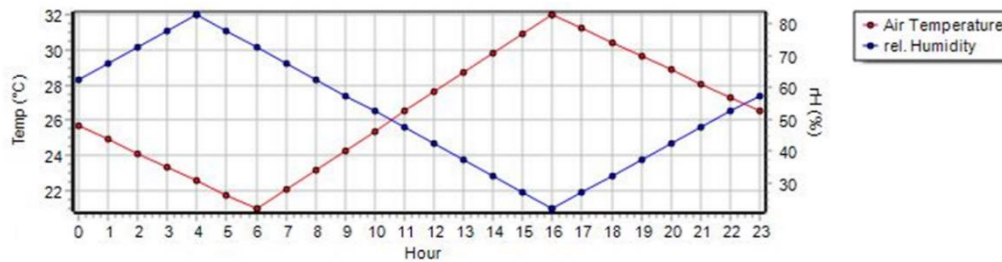


Figure 4. Variation in the air temperature and the relative humidity during the day, extracted from the meteorological input data interface of the ENVI-Met software.

Table 3 summarizes the climatic inputs from the meteorological archives.

Table 3. Input data in the ENVI-Met simulation model.

Climatic Variable	15 July 2021			
	Min	Time of Min	Max	Time of Max
Air temperature	21 °C	06:00 a.m.	32 °C	04:00 p.m.
Relative humidity	22%	04:00 p.m.	83%	04:00 a.m.
Constant Windspeed	3.00 m/s		Direction	West

Since the existing model and the meteorological input data are the same ones that the authors have implemented in a recent microclimate analysis, the validation procedure [62] and its results coincide with [39]. The simulation provides several climatic outputs: in this study, the comparison between the scenarios focuses on AT, MRT, and PMV.

MRT quantifies the effect of environmental radiation on the human body, and it is widely used in external thermal environments and thermal comfort studies [63–65]. ENVI-Met performs detailed heat transfer simulations between the surfaces of the model, achieving good results, as reported in the literature [66–68]. The software calculates MRT using Equation (1):

$$MRT^4 = \sum_{i=1}^N T_i^4 F_{p \rightarrow i}, \tag{1}$$

where i is the indicator of the N surrounding surfaces, T_i is the temperature of the surrounding surfaces, and $F_{p \rightarrow i}$ are view factors between the person and the whole surrounding environment.

PMV is a human comfort index that allows ex ante and ex post analyses for the evaluation, design, and control of thermal environments according to [69]. In this study, the reference man is 35-year-old, 1.75 m tall, and weighs 75 kg. According to Equation (2) [70], PMV summarizes the physical and physiological parameters allowing a correlation between thermal comfort and meteorological parameters:

$$PMV = (0.303 \exp - 0.0336M + 0.028) \times \{(M - W) - 3.5 \times 10^{-3} \times [5733 - 6.99 \times (M - W) - p_a] - 0.42 \times (M - 58.5) - 1.7 \times 10^{-5} \times M \times (5867 - p_a) - 0.0014 \times M \times (34 - t_a) - 3.96 \times 10^{-8} \times f_{cl} \times [(t_{cl} + 273)^4 - (t_r + 273)^4] - f_{cl} \times h_c \times (t_{cl} - t_a)\} \tag{2}$$

where M is the metabolism rate, W is the external work, p_a is the partial water vapor pressure (Pa), t_a is the air temperature ($^{\circ}\text{C}$), f_{cl} is the surface area factor of clothing, t_{cl} is the surface temperature of clothing ($^{\circ}\text{C}$), t_r is the mean radiant temperature ($^{\circ}\text{C}$), and h_c is the convective heat transfer coefficient ($\text{W}/(\text{m}^2 \times \text{K})$). Three conditions are defined, depending on the PMV values:

- Ideal conditions (IC) for a range of values ± 1 ;
- Acceptable conditions (AC) for values between $(-3, -1)$ and $(1, 3)$;
- Critical conditions (CC) for values over ± 3 .

Figure 5 shows an extreme daily pattern of PMV because it achieves both hot and cold critical conditions. In this study, the calculation of the different colored areas in the figure identifies the best road pavement to guarantee a good state of thermal comfort. Specifically, the best strategy is the one that presents the smallest CC areas.

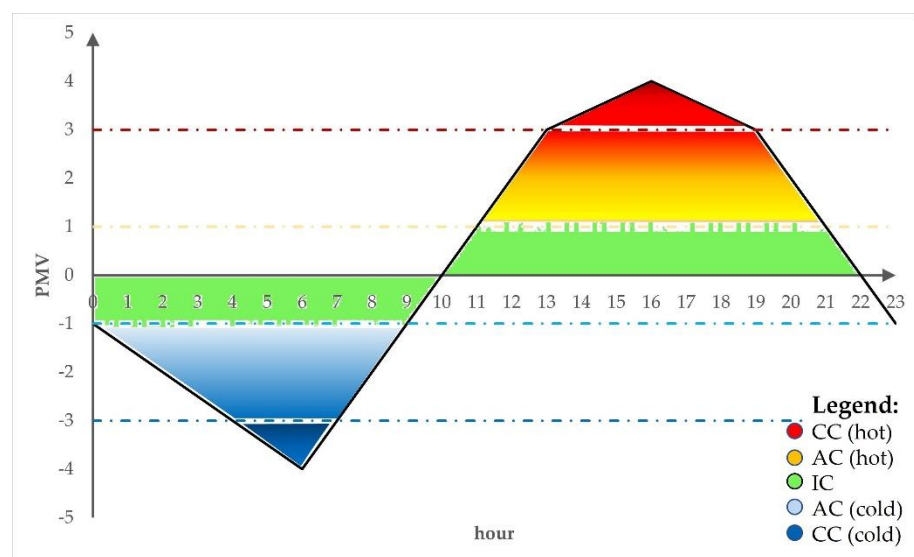


Figure 5. Example of an extreme daily trend of the PMV.

3. Results

Figure 6a shows a 2D visualization of the model: buildings and walls of different heights surround the parking area, as shown in Figure 6b. Both figures display the location of nine receptors ($R_i, i = 1, \dots, 9$) within the parking area, whose thermal performances have been investigated.

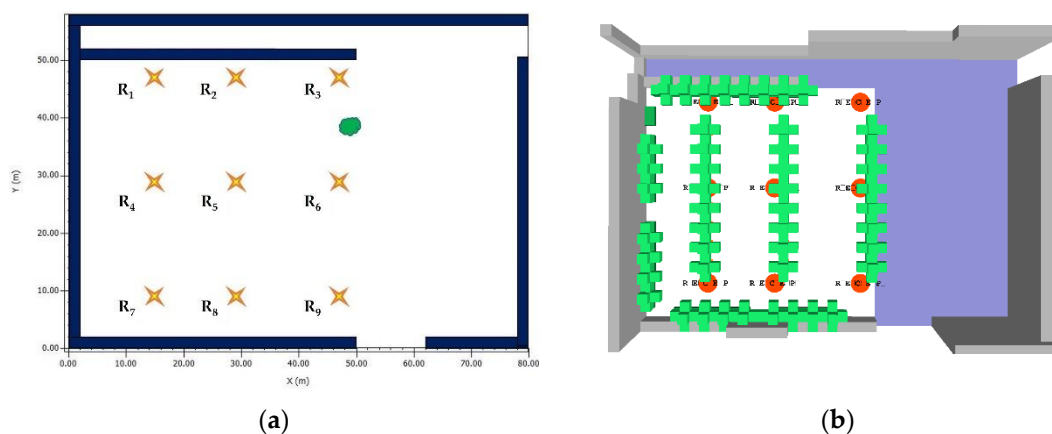


Figure 6. Layout of the ENVI-Met model and the receptors: (a) 2D visualization; (b) 3D visualization.

The microclimatic investigation was carried out in terms of AT, MRT, and PMV, evaluating the above parameters for all four of the scenarios analyzed in the hottest month of the year. The Results section is divided into three subheadings, one for each investigated parameter, in which the obtained results are analyzed in detail.

3.1. AT Results

Focusing on AS, a statistical evaluation of AT was performed in terms of the maximum, minimum, and average AT (T_{\max} , T_{\min} , and T_{avg} , respectively), and the standard deviation (σ) values of AT. Table 4 shows the results from the hottest hours during the day.

Table 4. Air temperature from 10:00 a.m. to 09:00 p.m. of 15 July 2021—Scenario AS.

Hour	AT (°C)									T_{\max} (°C)	T_{\min} (°C)	T_{avg} (°C)	σ (°C)
	R ₁	R ₂	R ₃	R ₄	R ₅	R ₆	R ₇	R ₈	R ₉				
10 a.m.	27.35	27.72	28.38	27.58	27.77	28.25	28.07	28.11	28.40	28.40	27.35	27.96	0.37
11 a.m.	28.46	28.86	29.63	28.50	28.71	29.25	28.85	28.87	29.20	29.63	28.46	28.93	0.38
12 a.m.	29.54	29.91	30.76	29.46	29.67	30.20	29.69	29.72	30.02	30.76	29.46	29.89	0.40
1 p.m.	30.38	30.81	31.70	30.18	30.48	31.02	30.41	30.48	30.78	31.70	30.18	30.69	0.46
2 p.m.	31.04	31.52	32.39	30.71	31.09	31.61	30.88	31.04	31.32	32.39	30.71	31.29	0.51
3 p.m.	31.61	32.09	32.91	31.07	31.60	32.08	31.19	31.49	31.74	32.91	31.07	31.75	0.55
4 p.m.	32.26	32.66	33.38	31.33	32.10	32.54	31.34	31.92	32.16	33.38	31.33	32.19	0.65
5 p.m.	31.62	31.90	32.61	30.94	31.64	32.07	30.92	31.53	31.82	32.61	30.92	31.67	0.53
6 p.m.	30.66	30.91	31.41	30.31	30.81	31.16	30.26	30.56	31.03	31.41	30.26	30.79	0.38
7 p.m.	29.77	29.92	30.17	29.56	29.86	30.08	29.55	29.77	30.03	30.17	29.55	29.86	0.22
8 p.m.	28.98	29.09	29.25	28.87	29.09	29.23	28.88	29.06	29.23	29.25	28.87	29.08	0.15
9 p.m.	28.28	28.37	28.48	28.27	28.45	28.55	28.31	28.47	28.60	28.60	28.27	28.42	0.12

At a fixed hour, the data in Table 4 highlight that there are no significant differences in terms of AT between the nine receptors: the differences between T_{\max} and T_{\min} are no more than 2 °C, and σ varies between 0.12 °C and 0.65 °C. Therefore, the authors focused their attention on three strategic receptors: R₅ is the central receptor in the parking lot; R₄ is shaded by trees in the new proposed scenarios (Figure 6b); and R₃ is never shaded in any of the simulated scenarios (Figure 6b). In addition, the comparison between the results was carried out at 12:00 a.m. (i.e., the time when the sun is at its zenith) and at 04:00 p.m. (i.e., the time with T_{\max}). Table 5 summarizes the AT comparison.

Table 5. AT values at 12:00 a.m. and 04:00 p.m.

Scenario	AT (°C) at 12:00 a.m.			AT (°C) at 04:00 p.m.		
	R ₃	R ₄	R ₅	R ₃	R ₄	R ₅
AS	30.76	29.46	29.67	33.38	31.33	32.10
LC+G1	28.78	27.69	27.67	31.63	30.28	30.45
LC+G2	28.79	27.70	27.67	31.59	30.24	30.40
LC+G3	27.68	26.87	27.13	30.59	29.75	29.97

According to Table 5, AS is the worst scenario because it has the highest AT values. Green furniture brings benefits due to the reduction in AT [71]. In detail, LC+G1 favors the abatement of AT of about 2 °C, while LC+G2 does not produce significant improvements compared to LC+G1. The best results are produced by LC+G3, in which the combination of 15 m high trees and the perimeter hedge ensures up to a 3 °C AT reduction compared to AS. In regards to R_i in the scenarios with light concrete pavement, the results depend on the shaded areas. In particular, R₄ has the lowest ATs, R₅ has intermediate ATs, and R₃ has the highest ATs. Figures 7a–d and 8a–d show the 2D colored maps of the AT trend at 12:00 a.m. and 04:00 p.m. for AS, LC+G1, LC+G2, and LC+G3, respectively.

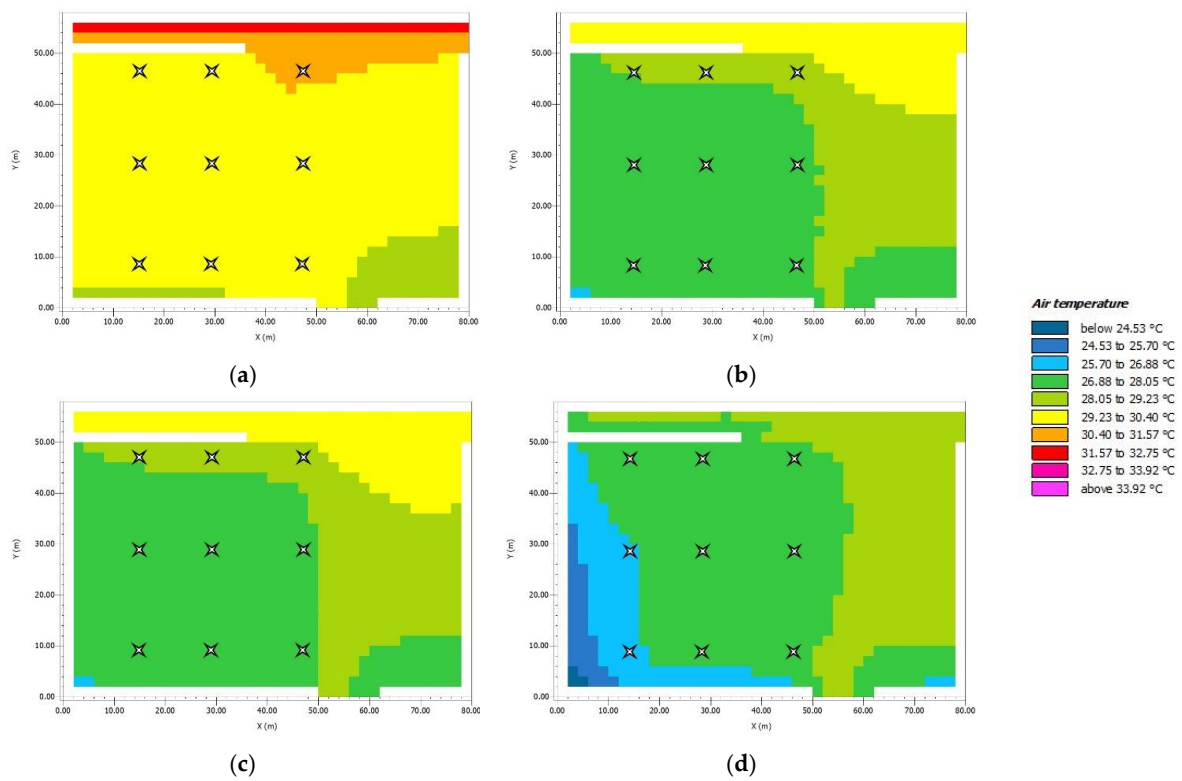


Figure 7. AT at 12:00 a.m. in July. (a) AS; (b) LC+G1; (c) LC+G2; (d) LC+G3.

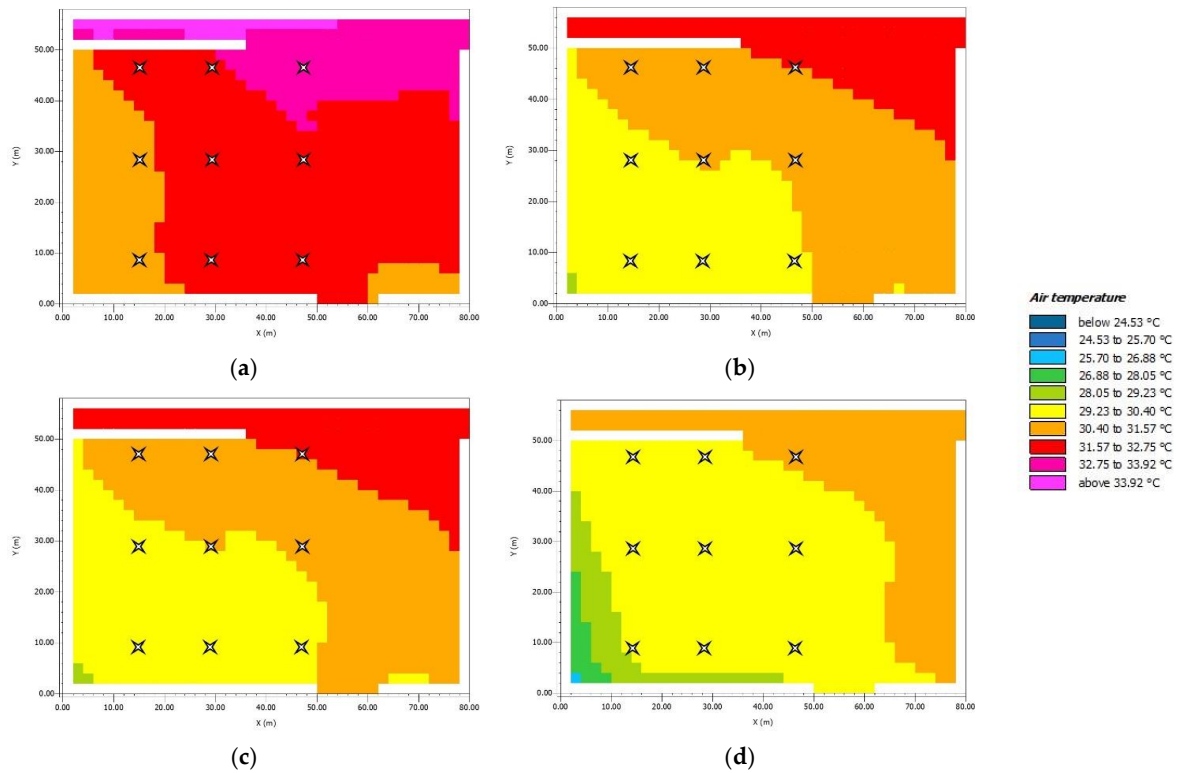


Figure 8. AT at 04:00 p.m. in July. (a) AS; (b) LC+G1; (c) LC+G2; (d) LC+G3.

Figures 7 and 8 confirm the data in Table 5. The overall view of the square shows that AS is the worst scenario (Figures 7a and 8a), while all the other ones with cool pavements imply an AT reduction due to the green furniture and produce an effective UHI mitigation.

3.2. MRT Results

Nevertheless, the study continues through the evaluation of MRT. Table 6 lists the values of MRT at 12:00 a.m. and 04:00 p.m. in R₃, R₄, and R₅.

Table 6. MRT values at 12:00 a.m. and 04:00 p.m.

Scenario	MRT (°C) at 12:00 a.m.			MRT (°C) at 04:00 p.m.		
	R ₃	R ₄	R ₅	R ₃	R ₄	R ₅
AS	62.45	62.06	61.84	64.53	43.54	64.00
LC+G1	67.09	60.52	62.79	65.33	47.73	67.21
LC+G2	66.31	59.38	61.77	64.60	46.70	66.40
LC+G3	39.31	40.79	40.93	32.37	33.19	33.35

Table 6 shows that LC+G3 is the best strategy in terms of MRT because it implies almost a 50% MRT reduction compared to AS due to UGIs. Therefore, a greater presence of greenery in the environment produces beneficial effects on human comfort, as the exchange in heat between man and the surrounding environment is reduced. Figures 9 and 10 show the MRT distribution over the square at 12:00 a.m. and 04:00 p.m., respectively. They confirm that AS is the worst scenario (Figures 9a and 10a), with an almost constant MRT value throughout the area due also to the absence of natural or artificial shelters. In the other scenarios, the benefits related to the denser greenery are appreciable. LC+G1 (Figures 9b and 10b) and LC+G2 (Figures 9c and 10c) show a discontinuity of the MRT trend near the trees and the perimeter hedge. LC+G3 (Figures 9d and 10d) records the best results due to 15 m high trees which cause an MRT reduction throughout the area. Moreover, the pairwise comparison between Figures 9a,d and 10a,d shows that the 50% MRT noted in Table 6 extends to the whole area.

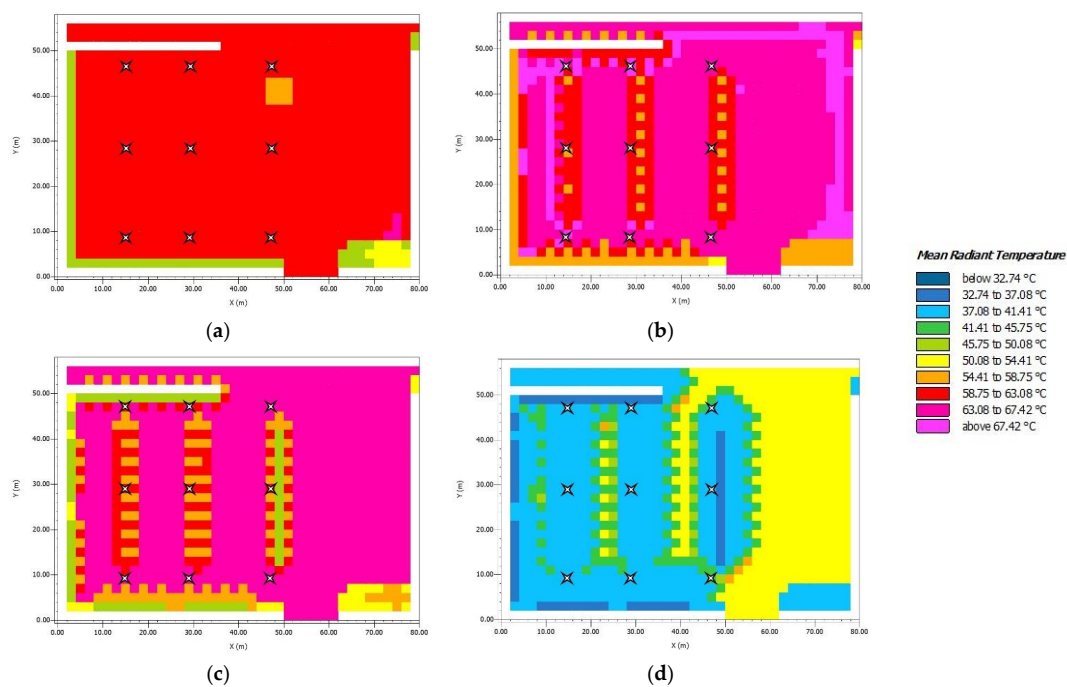


Figure 9. MRT at 12:00 a.m. in July. (a) AS; (b) LC+G1; (c) LC+G2; (d) LC+G3.

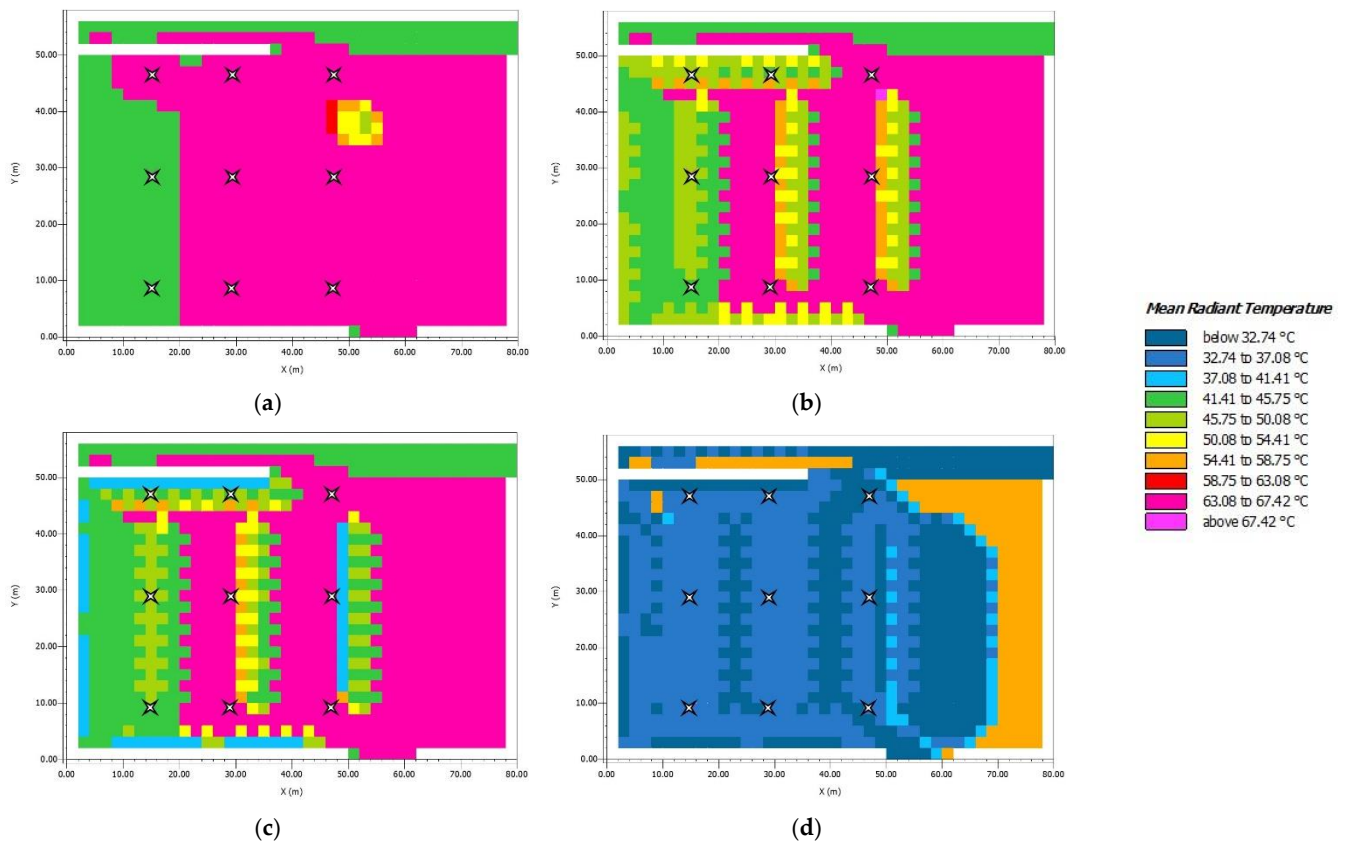


Figure 10. MRT at 04:00 p.m. in July. (a) AS; (b) LC+G1; (c) LC+G2; (d) LC+G3.

3.3. PMV Results

Finally, Figure 11 shows the daily PMV curves of R_5 for all the scenarios. The CC, AC, and IC thresholds allow us to observe the extension of the four trends in the different strips.

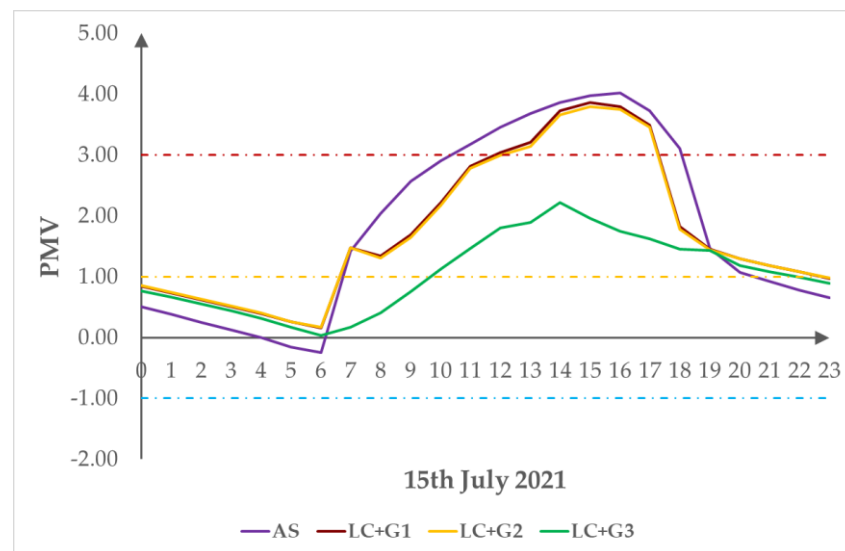


Figure 11. Daily PMV curves of R_5 .

The overlapping daily PMV trends in Figure 11 highlight that LC+G3 is the best strategy: the LC+G3 curve never exceeds the critical threshold (CC), which has a PMV value of 3. Furthermore, Figures 12 and 13 show the PMV distribution on the square at 12:00 a.m. and 04:00 p.m., respectively.

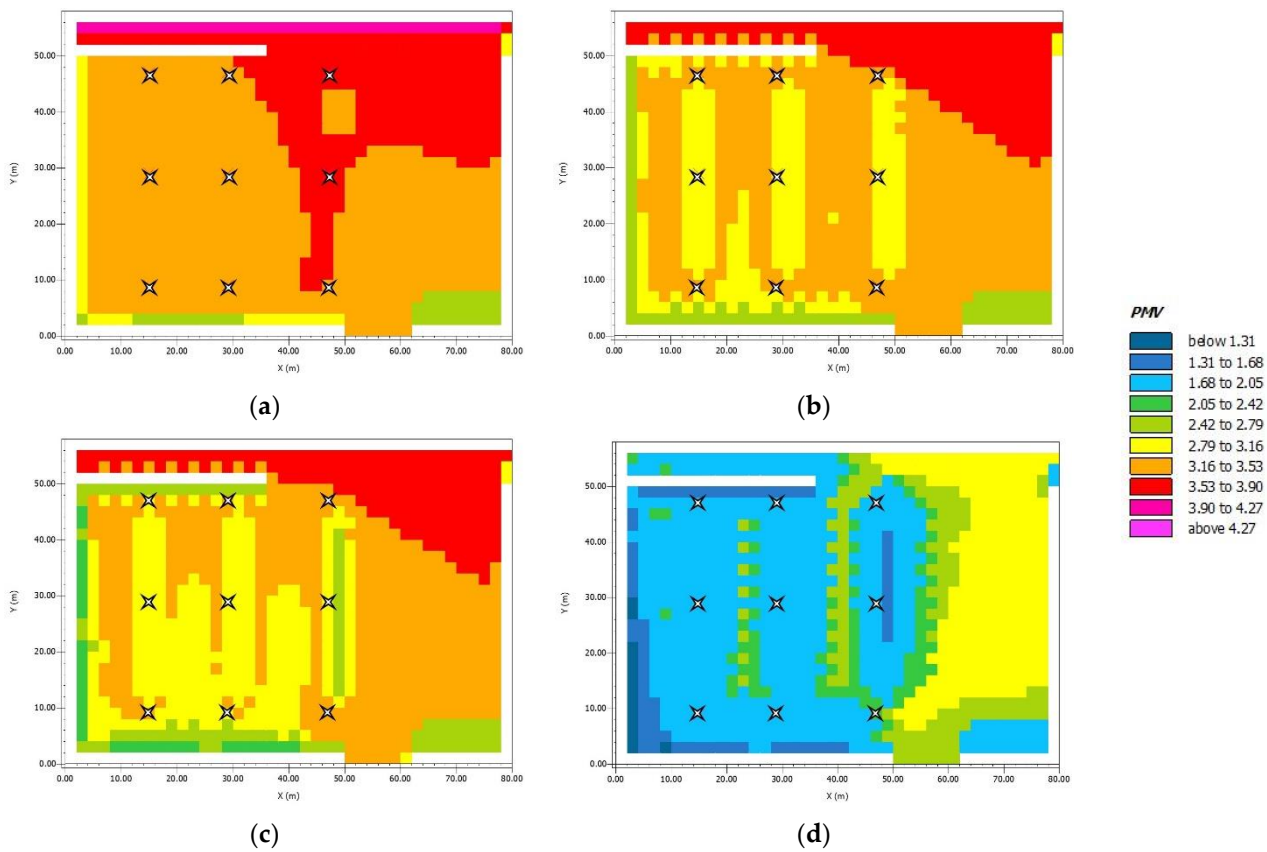


Figure 12. PMV at 12:00 a.m. in July. (a) AS; (b) LC+G1; (c) LC+G2; (d) LC+G3.

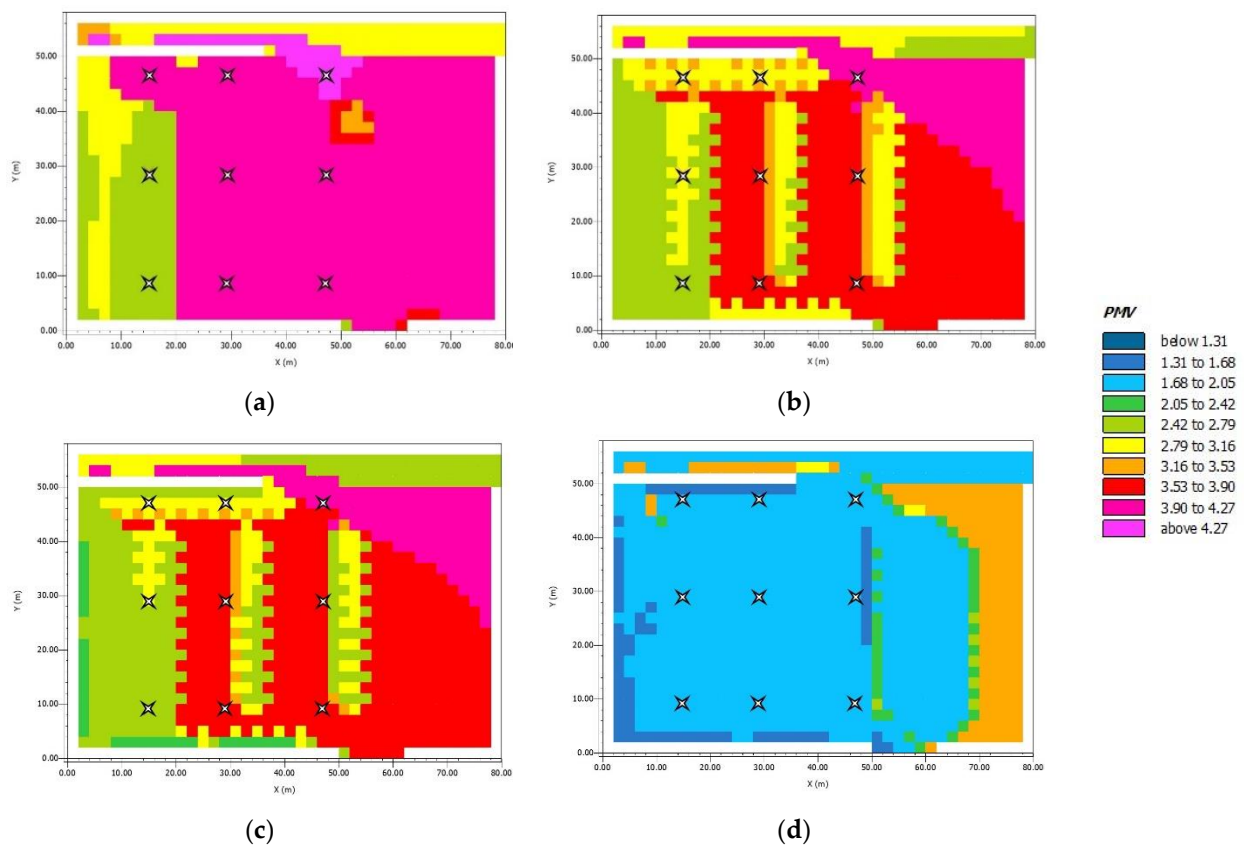


Figure 13. PMV at 04:00 p.m. in July. (a) AS; (b) LC+G1; (c) LC+G2; (d) LC+G3.

In Figures 12 and 13, all the proposed scenarios provide better results than AS. In detail, LC+G1 (Figures 12b and 13b) and LC+G2 (Figures 12c and 13c) have a similar distribution of PMV values near the green areas. LC+G3 has excellent results (Figures 12d and 13d), in which the PMV is significantly reduced for the whole square. In detail, the west parking area, where the green furniture is, has almost a constant trend of PMV and reaches its minimum value. On the other hand, the east sampietrini pavement causes greater PMV values which, however, are lower than AS. This last observation confirms that greenery and trees bring benefits to the whole square.

For a more detailed analysis, the authors adopted the methodology they proposed in [39] to quantify the exposure time of the examined square to the comfort condition strips in Figure 5 throughout a 24 h period. The results in Table 7 allow a direct quantitative comparison between the scenarios.

Table 7. PMV daily analysis of July.

Scenario	Receptor	$PMV \leq -3$ ($PMV \times h$)	$-3 < PMV < -1$ ($PMV \times h$)	$-1 \leq PMV \leq 1$ ($PMV \times h$)	$1 < PMV < 3$ ($PMV \times h$)	$PMV \geq 3$ ($PMV \times h$)
AS	R ₃	0.00	0.00	16.81	21.02	6.94
	R ₄	0.00	0.00	17.24	18.95	2.69
	R ₅	0.00	0.00	17.42	21.38	4.92
LC+G1	R ₃	0.00	0.00	16.57	20.09	4.75
	R ₄	0.00	0.00	19.58	19.01	0.57
	R ₅	0.00	0.00	19.76	18.40	2.91
LC+G2	R ₃	0.00	0.00	16.57	19.93	4.49
	R ₄	0.00	0.00	19.60	18.62	0.35
	R ₅	0.00	0.00	19.81	18.16	2.64
LC+G3	R ₃	0.00	0.00	16.28	8.89	0.00
	R ₄	0.00	0.00	17.38	6.14	0.00
	R ₅	0.00	0.00	17.37	6.95	0.00

Table 7 confirms that the existing AS is the worst scenario because it has the highest exposure to CC (6.94 $PMV \times h$ in R₃). LC+G1 and LC+G2 are very similar in terms of PMV (4.75 $PMV \times h$ and 4.49 $PMV \times h$ in R₃, respectively). Their results prove that the hedge is not enough to obtain high benefits. Instead, the high trees in LC+G3 ensure that this strategy is the best one to counteract UHI, since the parking area is never in critical conditions (0.00 $PMV \times h$ in R₃). In addition, LC+G3 presents low AC results (about 30% compared to those of the other scenarios) and its longest exposure is under ideal conditions (16.28 $PMV \times h$ in R₃).

4. Discussion

In this article, the authors carried out a microclimatic investigation to assess the current thermal conditions of an Italian square in the historic center of Rome and counteract the negative effects of UHI [72]. The existing condition has been compared to three scenarios obtained by replacing the road asphalt pavement with light concrete and inserting variable greenery [73]. The meteorological input data derive from weather archives. However, the constant wind speed and simplified diurnal cycles of temperature and relative humidity (Table 3) are due to the limitations of data handling by the model. Moreover, the lack of a diurnal cycle in the albedo, as well, as the single value of emissivity (Table 1), is a limitation in the ENVI-Met model. The current configuration implemented in ENVI-Met has been validated to prove the reliability of the study [72,74]. Then the simulated scenarios have been compared in terms of AT, MRT, and PMV in the hottest month of the year.

The results showed that the use of cool pavements and green furniture produces interesting results for all the analyzed variables [75]:

- In terms of AT, the three proposed scenarios have similar and comparable results. They ensure an AT abatement of 2–3 °C compared to the current state of the examined area. In the hottest hour of the day (i.e., 04:00 p.m.), AT decreases from the current value of 32.10 °C to 29.97 °C of LC+G3;
- The MRTs show that LC+G3 is the most comfortable solution (from the current 64.53 °C to 32.37 °C) [76]. LC+G3 shows a 50% reduction in MRT due to the 15 m high trees that shade the area [77]. Indeed, MRTs of LC+G1 and LC+G2 (65.33 °C and 64.6 °C) differ by few degrees from AS, showing that the shade from the 5 m high trees does not significantly reduce the heat exchange. The results in terms of PMV comply with MRTs. In Figure 11, the maximum PMV values of AS, LC+G1, and LC+G2 are 4.02, 3.86, and 3.80, respectively. They do not significantly differ in the hottest hour despite the different characteristics of the pavement and the green furniture [78];
- The quantitative analysis over 24 h of PMV disproves what was previously noted at 4 p.m. because LC+G1 and LC+G2 imply a shorter exposure to the worst condition (CC) than AS (Table 7). LC+G3 is confirmed to be the best solution even in terms of PMV. Its maximum PMV value is 2.22 and it is not exposed to critical conditions during the day [79].

According to the examined variables, LC+G3 combining cool pavement (i.e., light concrete) and green furniture (i.e., 15 m trees and hedge) is the best scenario. However, it cannot be overlooked that LC+G3 can be achieved only in the long run due to the height of the trees.

The proposed study confirms the data in the literature [80]: the UHIs depend on different aspects, such as road pavements, the thermal properties of the materials adopted, and the local conditions of the specific site, such as its LAT/LONG location on which the intensity of solar radiation and the buildings surrounding the area examined depend [81]. Therefore, the meteorological, geographical, and geometrical characteristics of the modeled site and the surrounding buildings affect the results, and their values apply in the case study. However, their trend is scalable to other contexts and cities (geographies).

5. Conclusions

In recent years, global warming has increasingly had serious consequences in terms of climate change. UHIs are caused by anthropization, with strong negative consequences for humans, which encourages people to produce even more pollution to combat them. Several scientific studies have shown how the use of green infrastructure (e.g., green roofs, green walls, green corridors, and green networks) and the replacement of existing road pavements with cool ones (e.g., stone, light concrete, and grass) improve the comfort level of humans. The proposed study performed a three-dimensional microclimatic analysis of Sts Peter in Chains' square (Rome, Italy) in July 2021 using ENVI-Met.

According to the Italian CAM, the authors propose new layouts for the modeled square by replacing the existing asphalt pavement in the parking lot with light concrete slabs and planting different green furniture and trees. In detail, LC+G1 has trees 5 m high in the parking area, LC+G2 has these as well as a perimeter hedge 1 m high, and LC+G3 has 15 m high trees and a perimeter hedge 1 m high. The comparison between the scenarios confirmed that the current scenario is the worst one, while the proposed strategies involve benefits, especially in terms of AT and PMV. The best scenario is LC+G3 because the higher trees with foliage shade larger areas. Compared to AS, LC+G3 results in a 3 °C AT reduction, a 50% MRT reduction, and comfortable conditions in terms of the maximum PMV value (2.22 compared to 4.02 of AS).

The results showed that great benefits could be obtained from the implementation of the different strategies proposed to counteract and mitigate the effects of UHIs. The use of a cool pavement made of light concrete and a good design of greenery gave the best results. Therefore, in an urban context, the redesign of public space can answer societal needs. For this purpose, further simulations will be carried out according to [37]. In particular, a grass layer and the light concrete pavement will be joined with photovoltaic surfaces

in the parking area to produce renewable energy for the increasing number of powered electric vehicles.

Author Contributions: Conceptualization, G.D.S., P.P. and L.M.; Formal analysis, G.D.S. and P.P.; Methodology, G.D.S. and L.M.; Software, P.P.; Validation, P.P. and L.M.; Writing—original draft, P.P.; Writing—review and editing, G.D.S., P.P. and L.M. All authors have read and agreed to the published version of the manuscript.

Funding: This research received no external funding.

Institutional Review Board Statement: Not applicable.

Informed Consent Statement: Not applicable.

Data Availability Statement: The data presented in this study are available on request from the corresponding author. The data are not publicly available due to confidentiality reasons.

Conflicts of Interest: The authors declare no conflict of interest.

References

- Enríquez-de-Salamanca, Á. Effects of Climate Change on Forest Regeneration in Central Spain. *Atmosphere* **2022**, *13*, 1143. [CrossRef]
- Paltsev, S.; Monier, E.; Scott, J.; Sokolov, A.; Reilly, J. Integrated Economic and Climate Projections for Impact Assessment. *Clim. Chang.* **2015**, *131*, 21–33. [CrossRef]
- Halder, B.; Bandyopadhyay, J. Evaluating the Impact of Climate Change on Urban Environment Using Geospatial Technologies in the Planning Area of Bilaspur, India. *Environ. Chall.* **2021**, *5*, 100286. [CrossRef]
- Indovina, F. *La Città Diffusa: Cos'è e Come Si Governa*; Daest-IUAV: Venice, Italy, 1989.
- Yang, J.; Wang, Z.H.; Chen, F.; Miao, S.; Tewari, M.; Voogt, J.A.; Myint, S. Enhancing Hydrologic Modelling in the Coupled Weather Research and Forecasting–Urban Modelling System. *Bound.-Layer Meteorol.* **2015**, *155*, 87–109. [CrossRef]
- Fathi, S.; Sajadzadeh, H.; Sheshkal, F.M.; Aram, F.; Pinter, G.; Felde, I.; Mosavi, A. The Role of Urban Morphology Design on Enhancing Physical Activity and Public Health. *Int. J. Environ. Res. Public Health* **2020**, *17*, 2359. [CrossRef]
- Faroughi, M.; Karimimoshaver, M.; Aram, F.; Solgi, E.; Mosavi, A.; Nabipour, N.; Chau, K.W. Computational Modeling of Land Surface Temperature Using Remote Sensing Data to Investigate the Spatial Arrangement of Buildings and Energy Consumption Relationship. *Eng. Appl. Comput. Fluid Mech.* **2020**, *14*, 254–270. [CrossRef]
- Mohajerani, A.; Bakaric, J.; Jeffrey-Bailey, T. The Urban Heat Island Effect, Its Causes, and Mitigation, with Reference to the Thermal Properties of Asphalt Concrete. *J. Environ. Manag.* **2017**, *197*, 522–538. [CrossRef] [PubMed]
- Halder, B.; Bandyopadhyay, J.; Khedher, K.M.; Fai, C.M.; Tangang, F.; Yaseen, Z.M. Delineation of Urban Expansion Influences Urban Heat Islands and Natural Environment Using Remote Sensing and GIS-Based in Industrial Area. *Environ. Sci. Pollut. Res.* **2022**, 1–24. [CrossRef]
- Moretti, L.; Di Mascio, P.; Fusco, C. Porous concrete for pedestrian pavements. *Water* **2019**, *11*, 2105. [CrossRef]
- Santamouris, M. Using Cool Pavements as a Mitigation Strategy to Fight Urban Heat Island—A Review of the Actual Developments. *Renew. Sustain. Energy Rev.* **2013**, *26*, 224–240. [CrossRef]
- Cantelli, A.; Monti, P.; Leuzzi, G. Influence of the Urban Heat Island Parameterization on Precipitation Forecasting in Limited Area Model. In *Environmental Hydraulics*; CRC Press: Boca Raton, FL, USA, 2010; Volume 2, pp. 1151–1156. [CrossRef]
- Ravanelli, R.; Nascetti, A.; Cirigliano, R.V.; Di Rico, C.; Leuzzi, G.; Monti, P.; Crespi, M. Monitoring the Impact of Land Cover Change on Surface Urban Heat Island through Google Earth Engine: Proposal of a Global Methodology, First Applications and Problems. *Remote Sens.* **2018**, *10*, 1488. [CrossRef]
- Cantelli, A.; Monti, P.; Leuzzi, G. An Investigation of the Urban Heat Island of Rome through a Canyon-Based Subgrid Scheme. *Int. J. Environ. Pollut.* **2011**, *47*, 239–247. [CrossRef]
- Khlystov, A.; Gualtieri, G.; Brilli, L.; Carotenuto, F.; Vagnoli, C.; Zaldei, A.; Gioli, B. Long-Term COVID-19 Restrictions in Italy to Assess the Role of Seasonal Meteorological Conditions and Pollutant Emissions on Urban Air Quality. *Atmosphere* **2022**, *13*, 1156. [CrossRef]
- Shahmohamadi, P.; Cubasch, U.; Sodoudi, S.; Che-Ani, A.I. Mitigating Urban Heat Island Effects in Tehran Metropolitan Area. In *Air Pollution—A Comprehensive Perspective*; Haryanto, B., Ed.; IntechOpen: London, UK, 2012. [CrossRef]
- Musco, F.; Fregolent, L.; Magni, F.; Maragno, D.; Ferro, D. *Calmierare gli impatti del fenomeno delle isole di calore urbano con la pianificazione urbanistica: Esiti e applicazioni del progetto Uhi (Central Europe) In Veneto*; JRC: Rome, Italy, 2014; ISBN 9788844806866.
- Tewari, M.; Yang, J.; Kusaka, H.; Salamanca, F.; Watson, C.; Treinish, L. Interaction of urban heat islands and heat waves under current and future climate conditions and their mitigation using green and cool roofs in New York City and Phoenix, Arizona. *Environ. Res. Lett.* **2018**, *14*, 034002. [CrossRef]
- Yang, J.; Wang, Z.H.; Kaloush, K.E.; Dylla, H. Effect of pavement thermal properties on mitigating urban heat islands: A multi-scale modeling case study in Phoenix. *Build. Environ.* **2016**, *108*, 110–121. [CrossRef]

20. Akbari, H.; Kolokotsa, D. Three Decades of Urban Heat Islands and Mitigation Technologies Research. *Energy Build.* **2016**, *133*, 834–842. [[CrossRef](#)]
21. Ranieri, V.; Coropulis, S.; Berloco, N.; Fedele, V.; Intini, P.; Laricchia, C.; Colonna, P. The Effect of Different Road Pavement Typologies on Urban Heat Island: A Case Study. *Sustain. Resil. Infrastruct.* **2022**, *1*, 153–168. [[CrossRef](#)]
22. Black-Ingersoll, F.; de Lange, J.; Heidari, L.; Negassa, A.; Botana, P.; Fabian, M.P.; Scammell, M.K. A Literature Review of Cooling Center, Misting Station, Cool Pavement, and Cool Roof Intervention Evaluations. *Atmosphere* **2022**, *13*, 1103. [[CrossRef](#)]
23. Kappou, S.; Souliotis, M.; Papaefthimiou, S.; Panaras, G.; Paravantis, J.A.; Michalena, E.; Hills, J.M.; Vouros, A.P.; Dimenou, K.; Mihalakakou, G. Cool Pavements: State of the Art and New Technologies. *Sustainability* **2022**, *14*, 5159. [[CrossRef](#)]
24. Moretti, L.; Loprencipe, G. Climate Change and Transport Infrastructures: State of the Art. *Sustainability* **2018**, *10*, 4098. [[CrossRef](#)]
25. Sangiorgio, V.; Fiorito, F.; Santamouris, M. Development of a Holistic Urban Heat Island Evaluation Methodology. *Sci. Rep.* **2020**, *10*, 17913. [[CrossRef](#)] [[PubMed](#)]
26. Cheela, V.R.S.; John, M.; Biswas, W.; Sarker, P. Combating Urban Heat Island Effect—A Review of Reflective Pavements and Tree Shading Strategies. *Buildings* **2021**, *11*, 93. [[CrossRef](#)]
27. Sanjuán, M.Á.; Morales, Á.; Zaragoza, A. Precast Concrete Pavements of High Albedo to Achieve the Net “Zero-Emissions” Commitments. *Appl. Sci.* **2022**, *12*, 1955. [[CrossRef](#)]
28. Kandelan, S.N.; Yeganeh, M.; Peyman, S.; Panchabikesan, K.; Eicker, U. Environmental Study on Greenery Planning Scenarios to Improve the Air Quality in Urban Canyons. *Sustain. Cities Soc.* **2022**, *83*, 103993. [[CrossRef](#)]
29. Nwakaire, C.M.; Onn, C.C.; Yap, S.P.; Yuen, C.W.; Onodagu, P.D. Urban Heat Island Studies with Emphasis on Urban Pavements: A Review. *Sustain. Cities Soc.* **2020**, *63*, 102476. [[CrossRef](#)]
30. Xu, C.; Chen, G.; Huang, Q.; Su, M.; Rong, Q.; Yue, W.; Haase, D. Can Improving the Spatial Equity of Urban Green Space Mitigate the Effect of Urban Heat Islands? An Empirical Study. *Sci. Total Environ.* **2022**, *841*, 156470. [[CrossRef](#)]
31. Ko, J.; Schlaerth, H.; Bruce, A.; Sanders, K.; Ban-Weiss, G. Measuring the Impacts of a Real-World Neighborhood-Scale Cool Pavement Deployment on Albedo and Temperatures in Los Angeles. *Environ. Res. Lett.* **2022**, *17*, 044027. [[CrossRef](#)]
32. Alves, F.M.; Gonçalves, A.; del Caz-Enjuto, M.R. The Use of Envi-Met for the Assessment of Nature-Based Solutions’ Potential Benefits in Industrial Parks—A Case Study of Argales Industrial Park (Valladolid, Spain). *Infrastructures* **2022**, *7*, 85. [[CrossRef](#)]
33. Perini, K.; Calise, C.; Castellari, P.; Roccotiello, E. Microclimatic and Environmental Improvement in a Mediterranean City through the Regeneration of an Area with Nature-Based Solutions: A Case Study. *Sustainability* **2022**, *14*, 5847. [[CrossRef](#)]
34. Zheng, T.; Qu, K.; Darkwa, J.; Calautit, J.K. Evaluating Urban Heat Island Mitigation Strategies for a Subtropical City Centre (a Case Study in Osaka, Japan). *Energy* **2022**, *250*, 123721. [[CrossRef](#)]
35. Romano, R.; Bologna, R.; Hasanaj, G.; Arnetoli, M.V. Adaptive Design to Mitigate the Effects of UHI: The Case Study of Piazza Togliatti in the Municipality of Scandicci. *Smart Innov. Syst. Technol.* **2020**, *163*, 531–541. [[CrossRef](#)]
36. Chatzinikolaou, E.; Chalkias, C.; Dimopoulou, E. Urban microclimate improvement using ENVI-met climate model. *Int. Arch. Photogramm. Remote Sens. Spat. Inf. Sci.* **2018**, *42*, 69–76. [[CrossRef](#)]
37. Italian Ministry of the Environment. *Adozione Dei Criteri Ambientali Minimi per l’Affidamento di Servizi di Progettazione e Lavori per la Nuova Costruzione, Ristrutturazione e Manutenzione di Edifici Pubblici*; Italian Ministry of the Environment: Rome, Italy, 2017.
38. Moretti, L.; Cantisani, G.; Carpiceci, M.; D’andrea, A.; Del Serrone, G.; Di Mascio, P.; Loprencipe, G. Effect of Sampietrini Pavers on Urban Heat Islands. *Int. J. Environ. Res. Public Health* **2021**, *18*, 13108. [[CrossRef](#)]
39. Moretti, L.; Cantisani, G.; Carpiceci, M.; D’Andrea, A.; Del Serrone, G.; Di Mascio, P.; Peluso, P.; Loprencipe, G. Investigation of Parking Lot Pavements to Counteract Urban Heat Islands. *Sustainability* **2022**, *14*, 7273. [[CrossRef](#)]
40. Di Mascio, P.; Moretti, L.; Capannolo, A. Concrete block pavements in urban and local roads: Analysis of stress-strain condition and proposal for a catalogue. *J. Traffic Transp. Eng.* **2019**, *6*, 557–566. [[CrossRef](#)]
41. Zoccali, P.; Moretti, L.; Di Mascio, P.; Loprencipe, G.; D’Andrea, A.; Bonin, G.; Teltayev, B.; Caro, S. Analysis of natural stone block pavements in urban shared areas. *Case Stud. Constr. Mater.* **2018**, *8*, 498–506. [[CrossRef](#)]
42. Acharya, T.; Riehl, B.; Fuchs, A. Effects of Albedo and Thermal Inertia on Pavement Surface Temperatures with Convective Boundary Conditions—A CFD Study. *Processes* **2021**, *9*, 2078. [[CrossRef](#)]
43. De Morais, M.V.B.; Guerrero, V.V.U.; de Freitas, E.D.; Marciotto, E.R.; Valdés, H.; Correa, C.; Agredano, R.; Vera-Puerto, I. Sensitivity of Radiative and Thermal Properties of Building Material in the Urban Atmosphere. *Sustainability* **2019**, *11*, 6865. [[CrossRef](#)]
44. Lopez-Cabeza, V.P.; Alzate-Gaviria, S.; Diz-Mellado, E.; Rivera-Gomez, C.; Galan-Marin, C. Albedo Influence on the Microclimate and Thermal Comfort of Courtyards under Mediterranean Hot Summer Climate Conditions. *Sustain. Cities Soc.* **2022**, *81*, 103872. [[CrossRef](#)]
45. Qin, Y.; Hiller, J.E.; Meng, D. Linearity between Pavement Thermophysical Properties and Surface Temperatures. *J. Mater. Civ. Eng.* **2019**, *31*, 04012962. [[CrossRef](#)]
46. Lu, Y.; Rahman, M.A.; Moore, N.W.; Golrokh, A.J. Lab-Controlled Experimental Evaluation of Heat-Reflective Coatings by Increasing Surface Albedo for Cool Pavements in Urban Areas. *Coatings* **2022**, *12*, 7. [[CrossRef](#)]
47. Wayne Lee, K.; Kohm, S. Cool Pavements as Sustainable Approaches for Green Streets and Highways. *Green Energy Technol.* **2014**, *204*, 439–453.
48. Di Maria, V.; Rahman, M.; Collins, P.; Dondi, G.; Sangiorgi, C. Urban Heat Island Effect: Thermal response from different types of exposed paved surfaces. *Int. J. Pavement Res. Technol.* **2013**, *6*, 414.

49. Aletba, S.R.O.; Abdul Hassan, N.; Putra Jaya, R.; Aminudin, E.; Mahmud, M.Z.H.; Mohamed, A.; Hussein, A.A. Thermal Performance of Cooling Strategies for Asphalt Pavement: A State-of-the-Art Review. *J. Traffic Transp. Eng.* **2021**, *8*, 356–373. [[CrossRef](#)]
50. O'Malley, C.; Kikumoto, H. An Investigation into Heat Storage by Adopting Local Climate Zones and Nocturnal-Diurnal Urban Heat Island Differences in the Tokyo Prefecture. *Sustain. Cities Soc.* **2022**, *83*, 103959. [[CrossRef](#)]
51. Zhang, T.; Zhao, X.; Zhao, Y.; Lukolongo, D.; Chabi, M.; Qi, F. Influences of Spherical Tree Canopy on Thermal Radiation Disturbance to Exterior Wall under the Condition of No Shade Cast on the Wall. *Build. Simul.* **2022**, *15*, 1367–1383. [[CrossRef](#)]
52. Li, L.; Zou, Z.; Zhou, T.; Zhou, X.; Li, Q. Simulation and Analysis of Influencing Factors of Pavement Thermal Environments in Guangzhou. *Sustainability* **2022**, *14*, 7251. [[CrossRef](#)]
53. Levinson, R.; Akbari, H. *Effects of Composition and Exposure on the Solar Reflectance of Portland Cement Concrete*; Elsevier: Amsterdam, The Netherlands, 2002; Volume 32. [[CrossRef](#)]
54. Abdulateef, M.F.; Al-Alwan, A.S.H. The Effectiveness of Urban Green Infrastructure in Reducing Surface Urban Heat Island. *Ain Shams Eng. J.* **2021**, *13*, 101526. [[CrossRef](#)]
55. Fahed, J.; Kinab, E.; Ginestet, S.; Adolphe, L. Impact of Urban Heat Island Mitigation Measures on Microclimate and Pedestrian Comfort in a Dense Urban District of Lebanon. *Sustain. Cities Soc.* **2020**, *61*, 102375. [[CrossRef](#)]
56. Asdrubali, F.; D'Alessandro, F.; Baldinelli, G.; Bianchi, F. Evaluating in Situ Thermal Transmittance of Green Buildings Masonries—A Case Study. *Case Stud. Constr. Mater.* **2014**, *1*, 53–59. [[CrossRef](#)]
57. Tseliou, A.; Koletsis, I.; Pantavou, K.; Thoma, E.; Lykoudis, S.; Tsiros, I.X. Evaluating the Effects of Different Mitigation Strategies on the Warm Thermal Environment of an Urban Square in Athens, Greece. *Urban Clim.* **2022**, *44*, 101217. [[CrossRef](#)]
58. Alsaad, H.; Hartmann, M.; Hilbel, R.; Voelker, C. ENVI-Met Validation Data Accompanied with Simulation Data of the Impact of Facade Greening on the Urban Microclimate. *Data Br.* **2022**, *42*, 108200. [[CrossRef](#)]
59. Tsoka, S.; Tsikaloudaki, A.; Theodosiou, T. Analyzing the ENVI-Met Microclimate Model's Performance and Assessing Cool Materials and Urban Vegetation Applications—A Review. *Sustain. Cities Soc.* **2018**, *43*, 55–76. [[CrossRef](#)]
60. Alvarez, I.; Quesada-Ganuza, L.; Briz, E.; Garmendia, L. Urban Heat Islands and Thermal Comfort: A Case Study of Zorrotzaurre Island in Bilbao. *Sustainability* **2021**, *13*, 6106. [[CrossRef](#)]
61. Fabbri, K.; Di Nunzio, A.; Gaspari, J.; Antonini, E.; Boeri, A. Outdoor Comfort: The ENVI-BUG Tool to Evaluate PMV Values Output Comfort Point by Point. *Energy Procedia* **2017**, *111*, 510–519. [[CrossRef](#)]
62. *ISO 7726-1998*; Ergonomics of the Thermal Environment-Instruments for Measuring Physical Quantities. International Organization for Standardization: Geneva, Switzerland, 1998.
63. Liu, K.; You, W.; Chen, X.; Liu, W. Study on the Influence of Globe Thermometer Method on the Accuracy of Calculating Outdoor Mean Radiant Temperature and Thermal Comfort. *Atmosphere* **2022**, *13*, 809. [[CrossRef](#)]
64. d'Ambrosio Alfano, F.R.; Ficco, G.; Frattolillo, A.; Palella, B.I.; Riccio, G. Mean Radiant Temperature Measurements through Small Black Globes under Forced Convection Conditions. *Atmosphere* **2021**, *12*, 621. [[CrossRef](#)]
65. Lukić, M.; Filipović, D.; Pecelj, M.; Crnogorac, L.; Lukić, B.; Divjak, L.; Lukić, A.; Vučićević, A. Assessment of Outdoor Thermal Comfort in Serbia's Urban Environments during Different Seasons. *Atmosphere* **2021**, *12*, 1084. [[CrossRef](#)]
66. Bruse, M.; Fleer, H. Simulating Surface-Plant-Air Interactions inside Urban Environments with a Three Dimensional Numerical Model. *Environ. Model. Softw.* **1998**, *13*, 373–384. [[CrossRef](#)]
67. Guo, H.; Aviv, D.; Loyola, M.; Teitelbaum, E.; Houchois, N.; Meggers, F. On the Understanding of the Mean Radiant Temperature within Both the Indoor and Outdoor Environment, a Critical Review. *Renew. Sustain. Energy Rev.* **2020**, *117*, 109207. [[CrossRef](#)]
68. Roth, M.; Lim, V.H. Evaluation of canopy-layer air and mean radiant temperature simulations by a microclimate model over a tropical residential neighbourhood. *Build. Environ.* **2017**, *112*, 177–189. [[CrossRef](#)]
69. *UNI EN ISO 7730:2006*; Ergonomia Degli Ambienti Termici-Determinazione Analitica e Interpretazione Del Benessere Termico Mediante Il Calcolo Degli Indici PMV e PPD e Dei Criteri di Benessere Termico Locale. UNI (Ente Italiano di Normazione): Milano, Italy, 2006.
70. *ASHRAE Standard 55-2017*; Thermal Environmental Conditions for Human Occupancy. ASHRAE: Atlanta, GA, USA, 2017.
71. Balany, F.; Ng, A.W.; Muttill, N.; Muthukumar, S.; Wong, M.S. Green Infrastructure as an Urban Heat Island Mitigation Strategy—A Review. *Water* **2020**, *12*, 3577. [[CrossRef](#)]
72. Ambrosini, D.; Galli, G.; Mancini, B.; Nardi, I.; Sfarra, S. Evaluating Mitigation Effects of Urban Heat Islands in a Historical Small Center with the ENVI-Met@Climate Model. *Sustainability* **2014**, *6*, 7013–7029. [[CrossRef](#)]
73. Massetti, L.; Petralli, M.; Orlandini, S. Effect of Green Areas on Summer Air Temperatures in Florence. In Proceedings of the ICUC8–8th International Conference on Urban Climates, Dublin, Ireland, 6–10 August 2012.
74. Liu, Z.; Cheng, W.; Jim, C.Y.; Morakinyo, T.E.; Shi, Y.; Ng, E. Heat Mitigation Benefits of Urban Green and Blue Infrastructures: A Systematic Review of Modeling Techniques, Validation and Scenario Simulation in ENVI-Met V4. *Build. Environ.* **2021**, *200*, 107939. [[CrossRef](#)]
75. Liang, T.C.; Wong, N.H.; Jusuf, S.K. Effects of vertical greenery on mean radiant temperature in the tropical urban environment. *Landsc. Urban Plan.* **2014**, *127*, 52–64.
76. Herrmann, J.; Matzarakis, A. Influence of mean radiant temperature on thermal comfort of humans in idealized urban environments. In Proceedings of the 7th Conference on Biometeorology, Freiburg, Germany, 12–14 April 2010; pp. 522–527.

77. Noro, M.; Lazzarin, R. Urban Heat Island in Padua, Italy: Simulation Analysis and Mitigation Strategies. *Urban Clim.* **2015**, *14*, 187–196. [[CrossRef](#)]
78. Li, Y.; Song, Y. Optimization of Vegetation Arrangement to Improve Microclimate and Thermal Comfort in an Urban Park. *Int. Rev. Spat. Plan. Sustain. Dev.* **2019**, *7*, 18–30. [[CrossRef](#)]
79. Bachir, N.; Bounoua, L.; Aiche, M.; Maliki, M.; Nigro, J.; El Ghazouani, L. The Simulation of the Impact of the Spatial Distribution of Vegetation on the Urban Microclimate: A Case Study in Mostaganem. *Urban Clim.* **2021**, *39*, 100976. [[CrossRef](#)]
80. Colter, K.; Middel, A.C.; Martin, C.A. Effects of Natural and Artificial Shade on Human Thermal Comfort in Residential Neighborhood Parks of Phoenix, Arizona, USA. *Urban For. Urban Green.* **2019**, *44*, 126429. [[CrossRef](#)]
81. Qian, Y.; Chakraborty, T.C.; Li, J.; Li, D.; He, C.; Sarangi, C.; Chen, F.; Yang, X.; Leung, L.R. Urbanization Impact on Regional Climate and Extreme Weather: Current Understanding, Uncertainties, and Future Research Directions. *Adv. Atmos. Sci.* **2022**, *39*, 819–860. [[CrossRef](#)]